TRIBOLOGICAL CHARACTERISATION OF POLYIMIDES UNDER ATMOSPHERIC CONDITIONS AT HIGH TEMPERATURE

P. SAMYN[1], P. DE BAETS[1], A. LEDDA[2], W. PHILLIPS[2]
Ghent University, Laboratory Soete[1] and TELIN[2], BELGIUM

SUMMARY

This work studies relations between sintered polyimide (SP-1) and its tribological properties under atmospheric conditions, where sliding experiments under controlled temperature between 100°C and 260°C are presently performed. As it has been recognised that wear debris contains extensive information about wear and friction mechanisms, two mathematical analysing techniques on generated wear debris are illustrated, the morphological pattern spectrum and the Fourier spectrum. Through image processing they can be used to extract parameters that relate to particle size and shape. Transitions in friction and wear can be further related to by aid of Raman spectroscopy applied on the worn polyimide surfaces.

1. INTRODUCTION

Polyimides are used in situations requiring high-performance plastics where other engineering materials do not function, because of their unique combination of superior mechanical, chemical and thermal properties. Pioneering research on the tribological behaviour of polyimides and its self-lubricating ability in film or bulk material has been performed by Fusaro [1] and Tewari and Bijwe, mainly under vacuum conditions used for space-applications. Although their studies show transitions in friction and wear mechanisms at higher sliding temperatures, the reasons for it remain difficult to illustrate and become more pronounced under atmospheric sliding conditions. It is believed that close examination of the wear debris and the worn polymer surface will provide additional information.

2. TRIBOLOGICAL EXPERIMENTS

Friction and wear tests are done on a cylinder-on-plate configuration in a PLINT TE 77 reciprocating test rig [2]. A line contact between the polyimide cylinder (Ø 6 mm x 15 mm) and the fixed steel counterface is applied. The initial contact is said to be counterformal, although it continuously grows as wear proceeds, called an ‘increasing contact area’ type of wear. A piezo-electrical force transducer is used to measure the friction force. The normal displacement of the cylinder towards its counterface is continuously measured by a contactless proximitor. Sliding temperatures are measured by a thermocouple positioned on top of the steel counterface, representing the average bulktemperature. An oscillating motion is provided by a controlled variable-speed motor through an excentric power transmission for adjustment of the stroke (15 mm). The sliding frequency is fixed at 10 Hz or 0.3 m/s. Different loads of 50 N, 100 N, 150 N and 200 N are applied. The steady-state contact pressure is geometrically calculated from the wear depth Δh. One test series is performed with free evolution of the contact temperature, only resulting from frictional heating. For other tests, the contact temperature can be regulated through constantly heating of the steel counterface at 100°C, 140°C, 180°C, 220°C and 260°C. Sintered polyimide Vespel SP-1 is used as unfilled base resin. Sintering polyimides after chemical reaction provides the polymer thermosetting characteristics. The counterface plates are made of hardened and tempered 40 CrMnNiMo8 steel (DIN 1.2738) with hardness of 300 HB and surface roughness $R_a = 0.10$ µm.

3. TEST RESULTS

3.1 Friction

The coefficients of friction are measured for different normal loads between 50 N and 200 N at variable sliding temperatures. After different sliding distances, the coefficient of friction is averaged, as plotted in Figure 1. Friction decreases progressively with increasing sliding distance towards a steady-state value that is obtained after approx. 4000 m of sliding. However, stabilisation occurs more difficult at higher temperatures. A transition in friction is found from 0.45 at temperatures below 180°C towards 0.25 for temperatures above 180°C. Under low loads (50 N) a characteristic peak in friction is found at 180°C before falling down.

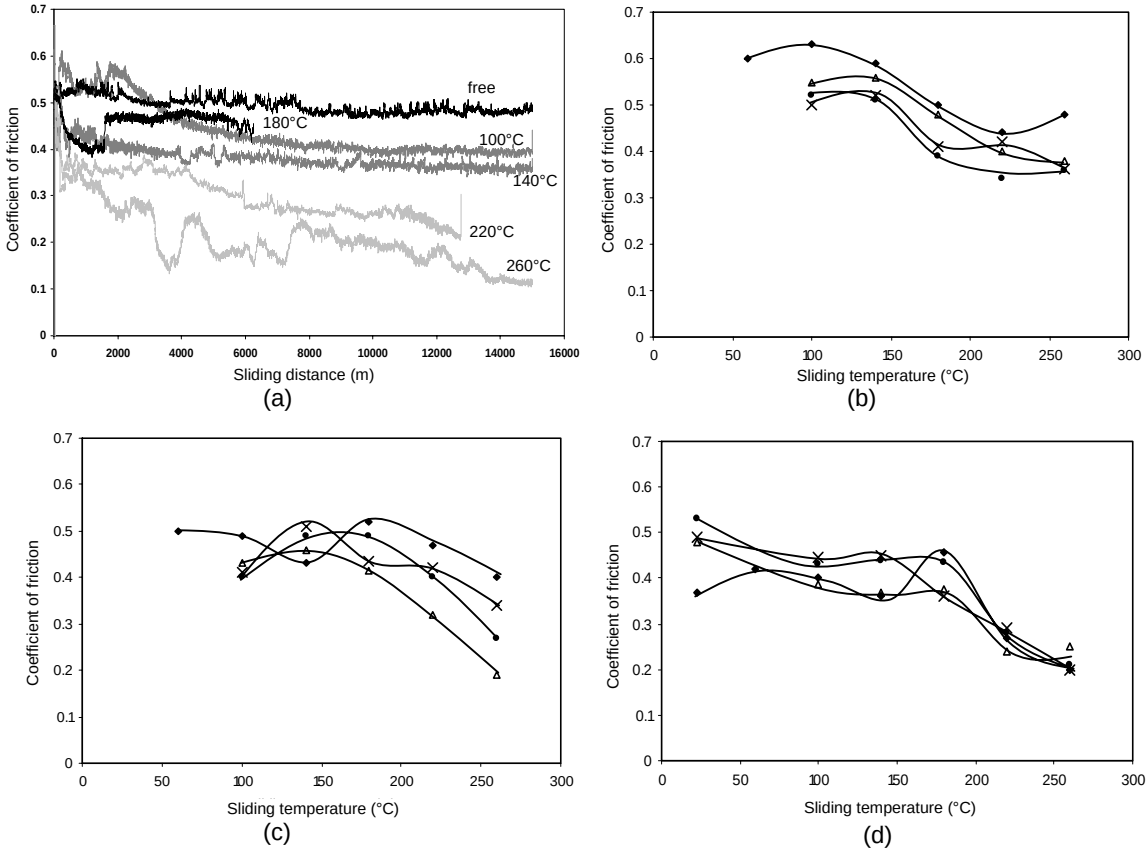

Figure 1. Coefficient of friction for different temperatures and normal loads
(a) graphs under 50 N, (b) after 30 m, (c) after 100 m, (d) after 8000 m or at the end of test
for normal loads of ♦ 50 N, Δ 100 N, ● 150 N and x 200 N

3.2 Temperature evolution in tests with 'free temperature'

Two temperature models are evaluated for the given contact situation with a rectangular moving heat-source (2ℓ x $2b$) under dry sliding. The length 2ℓ is measured in the direction of sliding and is geometrically calculated from the regime wear depth of the polyimide cylinder, while $2b$ is measured perpendicular to the direction of sliding and equals 15 mm. The generated frictional heat $q = \mu F_N v$, where F_N is taken equal to the normal load and v the sliding velocity. According to Loewen and Shaw [3] the maximum and mean rise in bulktemperature at the sliding interface are given by Formula (1), with A_{max} and $\bar{A}$ the area factors, given as a function of the aspect ratio of the surface area (b/ℓ). A second temperature model according to Jaeger [4] may be applied for estimating the flash temperatures according to Formula (2), with F_N (normal load), v (sliding velocity), 2ℓ (length in direction of sliding, geometrically calculated from wear depths Δh) and k (thermal conductivity of sliding bodies), added to 25°C ambient temperature.

$$\theta_{max} = A_{max}\frac{q\ell}{k} \quad , \bar{\theta} = \bar{A}\frac{q\ell}{k} \quad (1) \qquad\qquad \theta_f = 0.236\frac{\mu F_N v}{2\ell\,(k_1+k_2)} + 25 \quad (2)$$

The maximum and mean bulktemperatures are calculated for the sliding tests with free temperature and are compared to experimental measured values in Figure 2, plotted as a function of the frictional power q = μ F_N v. There is a good correlation between measured and calculated bulk- and flashtemperatures, however they remain below 100°C and higher temperatures artificially implied in temperature-controlled tests effects friction and wear properties.

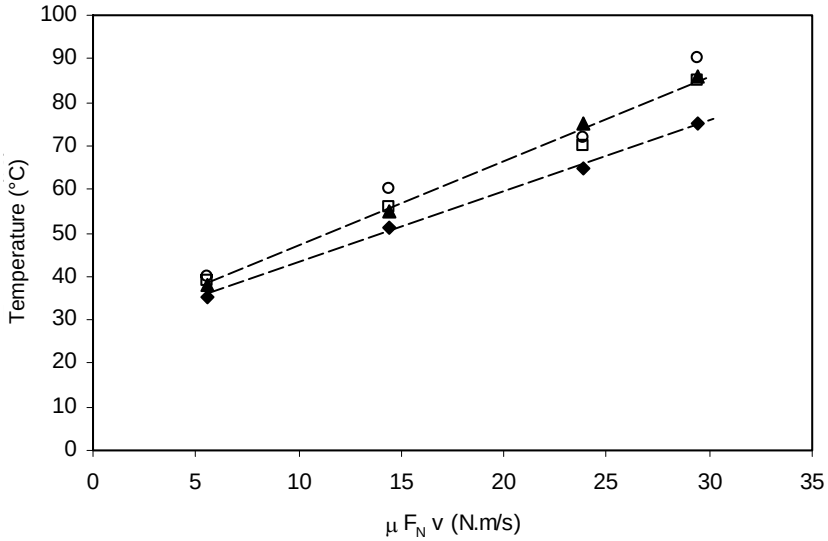

Figure 2. Calculated and measured bulk- and flash- temperatures
(♦ $\bar{\theta}$, ▲ θmax, and □ θf calculated temperatures, ○ measured temperatures)

3.3 Wear

Most of the small-scale tests under controlled atmosphere show linearly increasing wear depths with sliding distance, only at temperatures of 220°C and 260°C there are revealed running-in effects with higher wear rates and a transition towards lower steady-state wear after certain sliding time. The polyimide volumetric wear rates based on weight measurements pertain to the total test period, and are shown in Figure 3. Wear rates show a decreasing trend towards 140°C and afterwards progressively increases. Under 50 N a maximum in wear occurs at 180°C, corresponding to the previously described peak-value in friction.

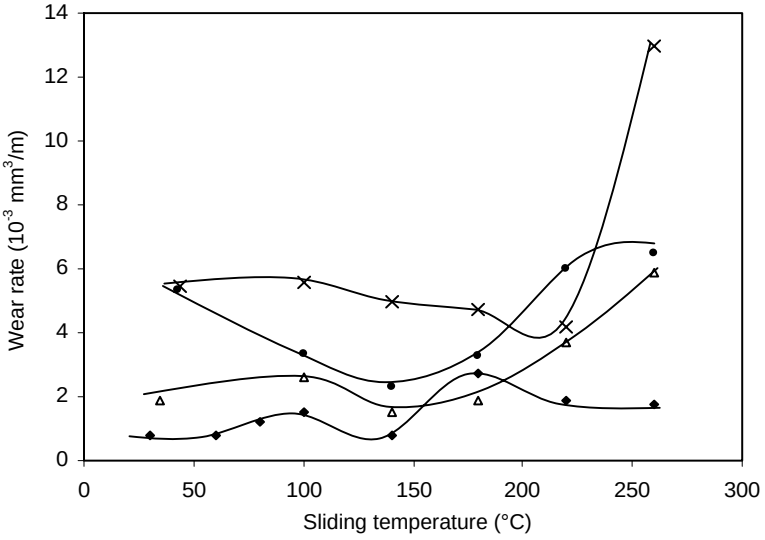

Figure 3. Volumetric wear rates for normal loads of ♦ 50 N, Δ 100 N, ● 150 N and x 200 N

4. DISCUSSION

4.1 Optical and SEM microscopy of steel counterface after sliding

Polyimide transfer films on the steel counterface ae studied by optical microscopy. In cases of free counterface temperature there is no evidence of polymer transfer. Also at controlled temperatures below 180°C no polymer transfer films is detected. As shown in Figure 4, only higher temperatures of 220°C and 260°C cause polymer transfer during the sliding test, where the formation of a transfer layer causes a transition from high running-in wear to lower steady-state wear. However, SEM-microscopy reveals that all of the transfer films remain discontinuous and in none of the cases a thin and homogeneous transfer film develops. The change in morphology of the wear surface reflects a change in friction and wear mechanisms. Also Fusaro [1] observed two different regions depending on the test conditions. The appearance of island and overall transfer regimes resembles spallation and brittle fracture respectively. Also he found transitions in friction and transfer mechanisms, attributing them to the higher polymer chain mobility and orientation effects at the surface in absence of water.

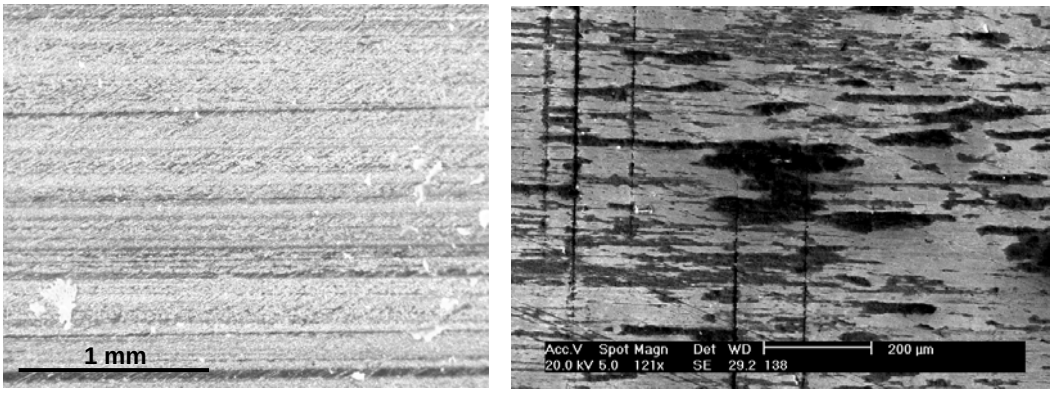

(a) (b)

Figure 4. Microscopy of steel counterfaces with polyimide transfer after sliding
(a) optical microscopy (100 N, 260°C), (b) SEM microscopy (200 N, 260°C)

4.2 Raman Spectroscopy of worn polyimide surfaces

The polyimide surfaces after sliding under 50 N at different sliding temperatures are characterised by Raman spectroscopy, measured on a Brucker FT spectrometer Equinox 55S. The spectrum of an unworn SP-1 specimen is shown in Figure 5. Characteristic absorption bands can be assigned to the C=C stretching vibration of the phenyl ring at 1612 cm^{-1} and 1513 cm^{-1} [5] and the C-N stretching vibration of the imide system at 1395 cm^{-1} and 1124 cm^{-1}. The C=O stretching in the imide ring is characterised by a band at 1786 cm^{-1}. The variation in relative intensity of some Raman bands as a function of sliding temperature is shown in Figure 6. The 1612 cm^{-1} peak is chosen as a reference band since it is correlated to the aromatic ring structure and has a central position. As such, it permits to demonstrate the relative orientation of functional groups. At higher temperatures, it is clear that the 1786 cm^{-1} peak grows progressively as the C=O group becomes more stretched. The bands at 1513 cm^{-1} and 1395 cm^{-1} show opposite trends with discontinuities at 180°C. They suggest that there is a reorientation of the functional groups depending on the sliding temperature. At 180°C there occurs an orientation of the aromatic phenylene ring that may become tilted parallel to the sliding surface, represented by the maximum value in the 1513 cm^{-1} band. This reorientation is confirmed by the maximum intensity of the 1601 cm^{-1} shoulder. It is also observed that at 180°C, the orientation of the C-N-C bonds is minimal. At higher temperatures, the latter functional group becomes more stretched. These opposite effects of both functional groups can explain the maximum in friction and wear that was observed for sliding under 50 N at 180°C.

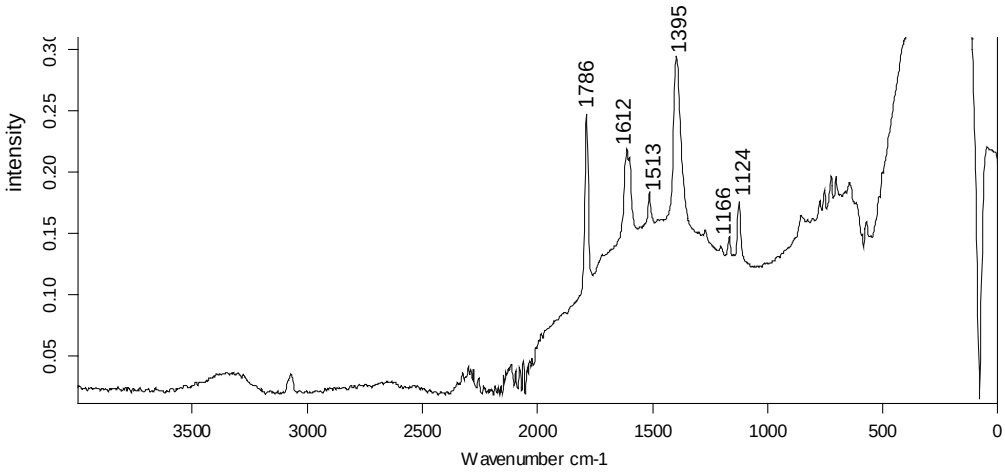

Figure 5. Example of Raman spectrum for an unworn polyimide SP-1 sample

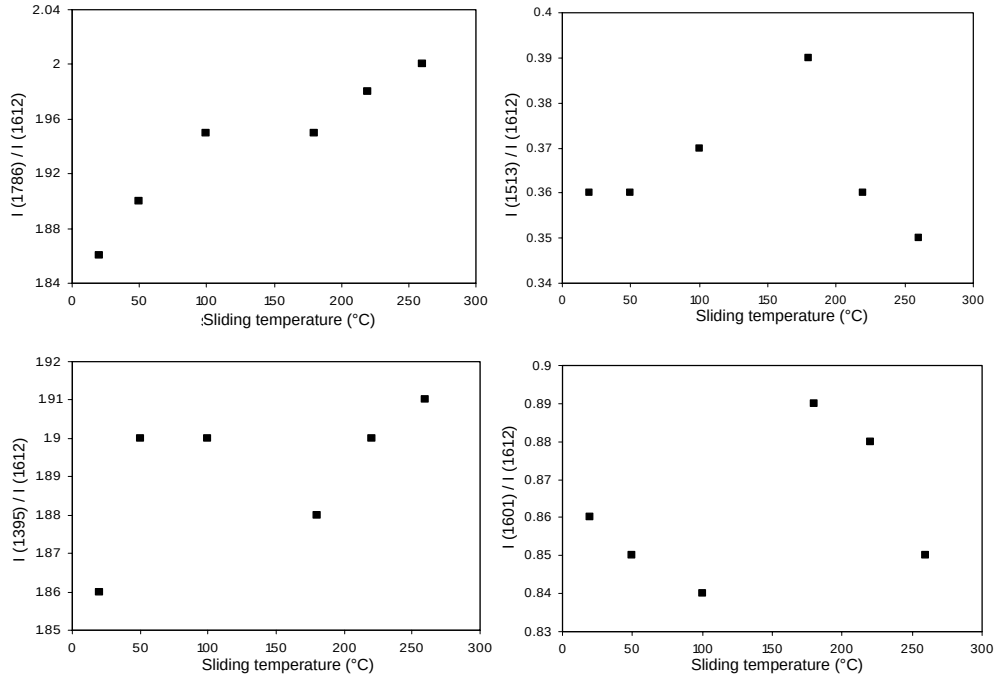

Figure 6. Evolution of the relative intensities of Raman bands as a function of sliding temperature, measured on the worn polyimide surfaces (50 N and controlled temperature)

4.3 Wear Debris Analysis

Photographs of wear particles as obtained by optical microscopy look like the ones in Figure 7. The original picturs were colour images with resolution 1300 x 1030, but they are converted into 8 bit grayscale pictures since the applied image processing algorithms as presented below only work on monochrome images.

a) Fourier Transform Analysis

The Fourier transform of an image results in an energy spectrum that reflects the grayscale periodicity in the image. Large image objects have low frequency values, while small objects are represented by the higher frequencies. Although the Fourier transform lacks the ability of spatial localisation, it is not a problem in present study since the debris particles are distributed randomly over the image and do not have to be localised. The size distribution of the particles should have it's effect on the shape of the Fourier spectrum. Images are transformed with the two dimensional Fast Fourier Transform (FFT) into a 2D-spatial frequency energy spectrum (Figure 8a). In order to calculate first-order histogram features and to remove the

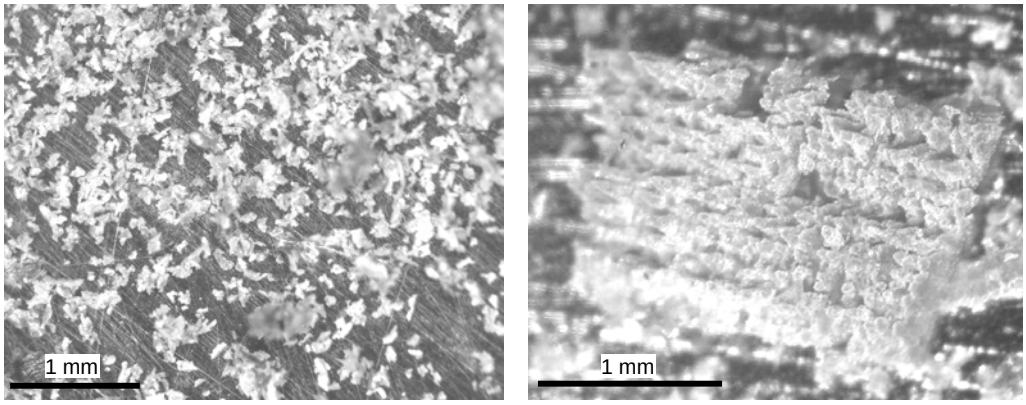

(a) (b)

Figure 7. Grayscale images of the debris particles of polyimide,
(a) Example to be further analysed by mathematical morphology (200 N, 260°C),
(b) Special features of large debris particles with porous structure (50 N, 260°C)

orientation dependency of the FFT-spectrum the 2D-spectrum is converted into a 1D-spectrun with on the abscissa the spatial frequency $\sqrt{\nu_x^2 + \nu_y^2}$. From this histogram, the parameters from Table 1 are computed, with b the histogram index and P(b) the value of histogram index b divided by the image area.

Table 1. Characteristic parameters computed from a Fast Fourier Transform histogram

Mean	**Standard deviation**	**Skewness**
$S_M = \bar{b} = \sum_b bP(b)$ Average histogram value	$S_D = \sigma_b = \left[\sum_b (b-\bar{b})^2 P(b)\right]^{1/2}$ Spread of the histogram values	$S_S = \frac{1}{\sigma_b^3}\sum_b (b-\bar{b})^3 P(b)$ Asymmetry of the histogram curve
Kurtosis	**Energy**	**Entropy**
$S_K = \frac{1}{\sigma_b^4}\sum_b (b-\bar{b})^4 P(b) - 3$ Curve shape relative to a normal distribution	$S_N = \sum_b P(b)^2$	$S_E = -\sum_b P(b)\log_2 P(b)$

b) Mathematical Morphology (Pattern Spectrum)

Mathematical morphology (MM) [6] is based on the set theory, where morphological operations simplify image data, preserving the objects' essential shape and size characteristics and eliminating irrelevant objects. The main advantage of a morphological filter for example is the ability to preserve the shape of large enough objects, unlike a Gaussian filter which blurs small and big objects indiscriminately. Two basic image operations are defined: *dilatation*, which fills holes and smoothens the contour lines of an object, and *erosion*, which removes small objects and disconnects objects connected by a small bridge. Such operations are defined in terms of a structuring element (strel), i.e. a small window that scans the image and alters the pixels in function of its window content. A dilatation of image A with strel B blows up the object, an erosion lets it shrink as illustrated in Figure 8b. If we take a strel B and perform an *opening* (an erosion followed by a dilatation) on an image A, some elements will disappear. If we take a bigger strel, then more elements in the image will vanish. In this way we can determine how the number of eliminated pixels increases when the image is morphologically opened using strels of increasing size.

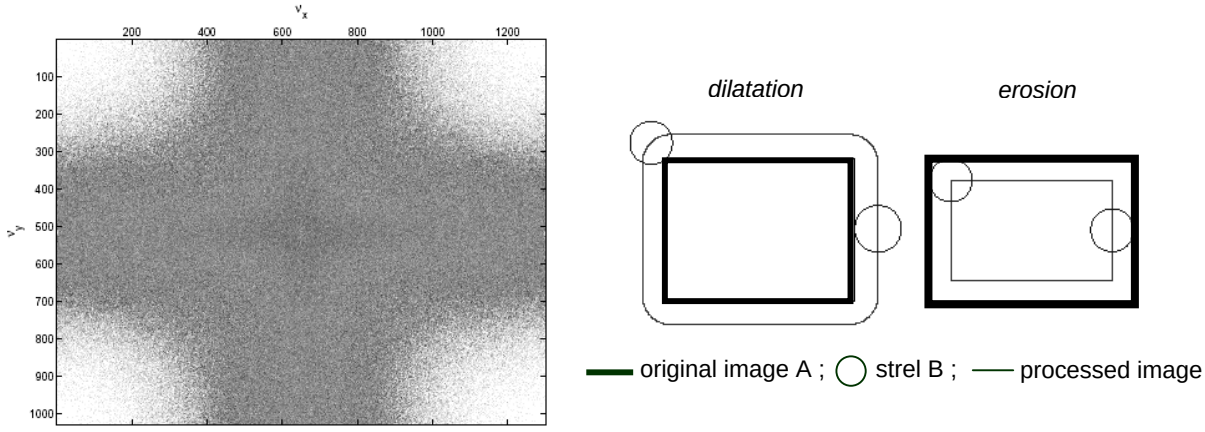

(a) (b)

Figure 8. Illustration of (a) FFT 2D-histogram and (b) image operations used for mathematical morphology

The resulting plot of the number of eliminated pixels versus the strel size n is called the pattern spectrum (PS) or the granulometric curve. As such, the pattern spectrum is a histogram of the distribution of the sizes of various objects displayed in an image. There is an analogy with the Fourier spectrum: the low frequencies in the Fourier spectrum relate to the global features of the image or the smooth objects, the high frequencies to the details or the fast grayscale variations. Similarly, big structuring elements in the pattern spectrum show the global features of the image or the large and smooth objects, while small sized strels also preserve the details or the small and rough image objects. From the pattern spectrum of image A with strels B of increasing size n, different parameters as in Table 2 can be distracted.

Table 3. Characteristic parameters computed from a Pattern Spectrum

Mean object size	**Entropy**
$S(A;B)=\frac{\sum_n nPS(A;B)(n)}{\sum_{a\in A}A(a)}$ area	$E(A;B)=-\frac{\sum_n PS(A;B)(n)\log_2\frac{PS(A;B)(n)}{\sum_{a\in A}A(a)}}{\sum_{a\in A}A(a)}$ quantification of the shape-size complexity
B-Shapiness	**N_{max}**
$BS(A;B)=\frac{PS(A;B)(N_{\max})}{\sum_{a\in A}A(a)}$ quantification of the resemblance of the objects to the strel shape	The last bin (the highest *n*-value, when all image objects are sieved out) of the pattern spectrum histogram

c) Results from image analysis

The correlation coefficients P between the different spectrum parameters and their respective experimental parameters (temperature and normal load) are given in Table 3. It also shows a value P', the probability of getting correlation as large as the observed value by random chance, when the true correlation is zero. So it is important for good correlation that the value for P is close to 1 and the value for P' is low. Since there are presently too few pictures available to do statistical analysis, the P' value will be quite large or lacks for temperature relationships since only two images were taken. However, there is a trend that temperature is proportional to the FFT mean and standard deviation, while normal load is inversely proportional to entropy at both 100°C and 180°C. For a pattern spectrum, temperature is inversely proportional to size and N_{max}, while load is proportional to entropy and N_{max}. Compared to FFT

histograms, there is observed a better correlation between the experimental parameters (temperature and normal load) and the characteristics from the pattern spectrum.

Table 3. Correlation coefficients for the FFT and PS spectra with the experimental parameters

Experimental parameters		Fast Fourier Transform histogram						Morphological Pattern Spectrum			
		S_M	S_D	S_S	S_K	S_N	S_E	S(A;B)	E(A;B)	BS(A;B)	N_{max}
Temperature F_N = 50 N	P	1	1	1	1	1	-1	-1	1	-1	-1
Temperature F_N = 100 N	P	1	1	-1	-1	-1	1	-1	-1	-1	-1
Temperature F_N = 150 N	P	1	1	1	1	-1	1	-1	-1	1	-1
Normal load T = 100 °C	P P'	-0.14 0.86	0.62 0.38	0.87 0.14	0.86 0.14	-0.009 0.99	-0.67 0.33	0.55 0.45	0.96 0.037	-0.79 0.21	0.88 0.12
Normal load T = 180°C	P P'	-0.83 0.38	-0.25 0.84	0.44 0.74	0.41 0.73	-0.94 0.23	-0.63 0.57	0.98 0.14	0.95 0.20	0.51 0.66	0.93 0.23

5. CONCLUSIONS

The influence of a controlled sliding temperature between 100°C and 260°C on friction and wear of sintered polyimides (Vespel SP-1) is investigated for different normal loads and fixed sliding velocity. Transitions in friction and wear are found in the region between 100°C and 200°C. Friction shows a decreasing trend above 180°C, while wear rates are minimal at 140°C. For the lowest test load (50 N) the wear rates go through a maximum value at 180°C in accordance with a peak value in friction.
By Raman spectroscopy it is demonstrated that the latter transitions at 180°C can be related to orientation effects of the phenylene ring and C-N-C bonds. With increasing temperature there is a continuously growing orientation of the C=O functional groups.
Collected wear debris is further analysed by two image processing techniques. It is illustrated that the Pattern Spectrum provides better correlation between spectrum parameters and experimental applied temperatures and loads than obtained from a Fast Fourier Transform histogram. However, more images than presently available should be analysed to fit good correlations between spectral analysis and tribological data.

6. REFERENCES

[1] R.L. Fusaro, Self-lubricating polymer composites and polymer transfer film lubrication for space applications, *Trib. Int., Vol. 23, No. 2 (1990), 105-121*

[2] P. Samyn, P. De Baets, G. Schoukens, B. Hendrickx, Tribological behaviour of pure and graphite-filled polyimides under atmospheric conditions, *Pol. Eng. Sci., Vol. 43, No. 8 (2003), 1477-1487*

[3] B. Bhushan, Principles and Applications of tribology, *Wiley-Interscience (1999), New York, ISBN 0-471-59407-5*

[4] C.J. Jaeger, Moving sources of heat and the temperature at sliding contacts, *Proc. Roy. Soc., NSW 76 (1942), 1107-1121*

[5] K.H. Yy, Y.H. Yoo, J.M. Rhee, M.H. Lee, S.C. Yu, Two-dimensional Raman correlation spectroscopy of the pathway for thermal imidization of Poly(amic acid), *Bull. Korean Chem. Soc., Vol. 24, No. 3 (2003), 357-362*

[6] P. Maragos, Pattern spectrum and multiscale shape representation, *IEEE Transactions on pattern analysis and machine intelligence, Vol. 11, No. 7 (1989), 701-716*